Ethylene Glycol Ions Dissociate by Tunneling through an H-Atom Transfer Barrier: A DFT and TPEPICO Study

Yue Li and Tomas Baer*

Department of Chemistry, University of North Carolina, Chapel Hill, North Carolina 27599-3290

Received: May 14, 2002; In Final Form: July 11, 2002

Density functional theory (DFT) and threshold photoelectron−photoion coincidence spectroscopy (TPEPICO) have been used to investigate the dissociation dynamics of the ethylene glycol ion. A total of 13 isomers of the ethylene glycol ion ($C_2H_6O_2^{+\bullet}$) and the transition states connecting them were obtained at the B3LYP/6-31G(d) level. The TPEPICO experimental results show that the $CH_3OH_2^+$ ion, produced by a double hydrogen transfer, and the CH_2OH^+ ion, produced by direct C−C bond cleavage, are the two dominant products. The H_2O loss channel, the lowest dissociation energy channel according to the DFT calculations, is suppressed because of a high barrier leading to its formation. The time-of-flight distributions of the $CH_3OH_2^+$ ion at low energies are asymmetric, which indicates that this ion is produced from a slowly dissociating (metastable) parent ion. A two-well−two-channel model is proposed to describe the isomerization and dissociation process. The simulations combined with RRKM theory suggest that the production of the $CH_3OH_2^+$ ion involves a hydrogen-bridged reaction intermediate, and its slow production is caused by tunneling through the isomerization barrier. This mechanism is supported by data for deuterated ethylene glycol. The 0 K appearance energy for the CH_2OH^+ ion is determined to be 11.08 ± 0.04 eV, from which the 298 K heat of formation of the ethylene glycol molecule is determined to be −383.1 ± 4.5 kJ/mol, in agreement with other experimental values.

Introduction

Ethylene glycol is one of the smallest prototypical bifunctional molecules, and its structure has been extensively studied experimentally (X-ray diffraction,[1] infrared spectroscopy,[2,3] and microwave spectroscopy[4−6]) and theoretically.[7−12] These studies indicate that the molecule prefers to adopt a gauche conformation, which is capable of forming an intramolecular hydrogen bond, making this conformation about 10 kJ/mol more stable than the trans isomer.

The photoelectron spectrum of the ethylene glycol molecule has been measured by several groups,[13−15] and the vertical ionization energy (IE) was accurately determined to be 10.55 eV. Early electron ionization (EI) studies[16−18] of the molecule reported the appearance energies (AE) of several fragment ions, CH_3O^+, $CH_2OH_2^{+\bullet}$, and $CH_3OH_2^+$. Among these, the production of the protonated methanol ion, $CH_3OH_2^+$, is interesting because it requires a double hydrogen atom transfer. Two mechanisms have been suggested for this reaction. In mechanism I (eq 1), neutral ethylene glycol in the hydrogen-bonded gauche conformation is ionized followed by a C−C bond cleavage and the simultaneous formation of a hydrogen-bridged intermediate. This is followed by a 1,5-hydrogen shift from one carbon atom to the other and the transfer of the hydrogen-bonded hydrogen atom to the ionic fragment. This mechanism is based on the mass spectrometric results of ethylene glycol and 2-methoxyethanol[19−21] and is also supported by the molecular orbital theoretical calculations of Burgers et al.[19]

However, on the basis of mass analyzed kinetic energy spectra (MIKES) of metastable ions with deuterated analogues of ethylene glycol and 2-methoxyethanol, Audier et al.[22] proposed

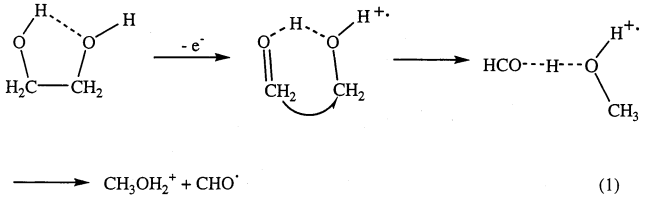

(1)

a different mechanism, which is shown in eq 2. Instead of only hydrogen atom transfers and a C−C bond rupture, the O−C−C−O backbone isomerizes to the C−O−C−C−O structure. That is, a new C−O bond is formed accompanying the cleavage of the C−C bond.

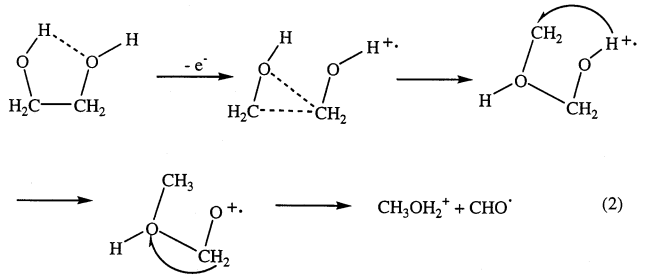

(2)

This mechanism accounts for the remarkable observation, based on collisional activation spectra of the product ions, that a hydroxylic hydrogen transfers to the carbon atom so that $DOCH_2CH_2OD^+$ dissociates at low energies exclusively to CH_2DOHD^+ and not $CH_3OD_2^+$ as would be the case with mechanism I. This observation effectively rules out mechanism I.

In an effort to test and to distinguish these mechanisms by other approaches, we have performed theoretical calculations on the potential energy surfaces of the above two mechanisms

* To whom correspondence should be addressed. E-mail: baer@unc.edu.

10.1021/jp021205s CCC: $22.00
Published on Web 08/20/2002

TABLE 1: Frequencies Used in the Energy Distribution and RRKM Rate Constant Calculations

$C_2H_6O_2$	174, 267, 330, 475, 532, 885, 901, 073, 1088, 1133, 1190, 1269, 309, 1402, 444, 1470, 1530, 539, 2997, 3005, 049, 3104, 3718, 3771
$C_2H_6O_2^{+\bullet}$(A)	137, 230, 376, 410, 505, 538, 878, 940, 1126, 146, 1164, 1252, 1278, 1298, 1396, 397, 1523, 1528, 3093, 3100, 3209, 224, 3659, 3669
$C_2H_6O_2^{+\bullet}$(B)	31, 94, 121, 150, 302, 330, 500, 877, 943, 1067, 150, 1185, 1332, 1479, 1506, 1509, 1728, 879, 2773, 2907, 3119, 3235, 3248, 3668
TS_{AB}	−1204,[a] 127, 282, 386, 399, 477, 597, 618, 82, 70, 1074, 1171, 1226, 1311, 1319, 461, 638, 688, 1804, 2413, 3025, 3161, 292, 3639
TS_{AB} (D_6)	−883,[b] 108, 264, 275, 359, 379, 480, 524, 703, 01, 837, 907, 950, 978, 1025, 1065, 191, 236, 1674, 1850, 2251, 2283, 2461, 2651
TS_{17}	−808,[c] 70, 161, 218, 262, 396, 502, 766, 960, 072, 1086, 1114, 1164, 1364, 1389, 449, 1494, 1604, 3160, 3171, 3304, 316, 3587, 3712
TS_B	−43,[a] 11, 16, 23, 52, 95, 206, 721, 821, 947, 136, 1170, 1289, 1477, 1493, 1502, 714, 1935, 2727, 3123, 3248, 3257, 591, 3673
TS_A	−33,[a] 20, 83, 121, 160, 241, 713, 751, 796, 820, 090, 1097, 1245, 1369, 1405, 1413, 1545, 565, 3181, 3190, 3337, 3338, 3668, 3685

[a] Reaction coordinate. The DFT calculated value for TS_{34} was 1720 cm^{-1}. [b] Reaction coordinate. The DFT calculated value for TS_{34} was 1262 cm^{-1}. [c] Reaction coordinate for mechanism 2. This is the DFT calculated value. The deuterated TS has a frequency of −748 cm^{-1}.

using density functional theory and carried out threshold photoelectron photoion coincidence (TPEPICO) studies on ethylene glycol and its deuterated analogue. Some structures in eq 1 have been obtained by Burgers et al.[19] However, we used a higher theory level (DFT) and larger basis sets (6-311+G-(d,p)) and calculated the transition states connecting the isomers.

Quantum Chemical Calculations

The calculations were performed on Origin 2000 computers at UNC−Chapel Hill and NC supercomputing center using a Gaussian 98 package.[23] Neutral and ionic species were fully optimized at the Hartree−Fock (HF) and DFT (B3LYP) levels using the 6-31G(d) basis set. The stationary points and first-order saddle points were confirmed through the calculation of harmonic vibrational frequencies, which were also used to obtain zero point vibrational energies (ZPE). To obtain more reliable energy results, single-point calculations were performed at the B3LYP/6-311+G(d,p) level using the B3LYP/6-31G(d) equilibrium geometries. The transition states were obtained using the synchronous transit-guided quasinewton (STQN) methods.[24,25] In the B3LYP calculations for all open shell species, the spin-squared expectation values, $\langle S^2 \rangle$, are close to 0.75, an ideal value for pure spin eigenstates; thus, spin contaminations can be ignored. For all transition states, intrinsic reaction coordinate (IRC) calculations were performed to determine the isomers or dissociation channels to which the transition states evolved.

Table S1 in the Supporting Information lists the energies, $\langle S^2 \rangle$, zero-point vibrational energies, and relative energies obtained at the different theory levels. The vibrational frequencies of neutral ethylene glycol molecule as well as those of some ions and transition states of importance to the TPEPICO data analysis are listed Table 1.

Experimental Approach

The TPEPICO apparatus has been described in detail previously.[26] Briefly, room-temperature sample vapor was leaked into the experimental chamber and ionized with vacuum ultraviolet (VUV) light from an H_2 discharge lamp dispersed by a 1 m normal incidence monochromator. The ions and the electrons were extracted in opposite directions with an electric field of 20 V/cm. The electrons detected by a channeltron electron multiplier and ions detected by a multichannel plate detector were used as start and stop pulses for measuring the ion time-of-flight (TOF). The TOF for each coincidence event was stored on a multichannel pulse height analyzer.

Two types of experiments were carried out. First, the fractional abundances of the precursor and product ions were measured as a function of the photon energy (breakdown diagram). Second, the product ion TOF distributions were measured at energies close to the dissociation limit of the precursor ion. Slowly dissociating (metastable) ions decay in the first acceleration region. The resulting product ion TOF distributions, which are asymmetrically broadened toward long TOF, can be analyzed to extract the ion dissociation rates as a function of ion internal energy.

The ethylene glycol sample ($C_2H_6O_2$, 99%, Aldrich) was used without further purification.

Results and Discussion

1. Quantum Chemical Calculations. 1.1. Structures of the $C_2H_6O_2^{+\bullet}$ Isomers and Transition States. The equilibrium structures along with some of the important bond distances (in angstroms) and bond angles (in degrees) for neutral ethylene glycol, 13 $C_2H_6O_2^{+\bullet}$ isomers, and transition states obtained at the B3LYP/6-31G(d) level are shown in Figure S1 of the Supporting Information. A comparison of the relative energies at the different levels (see Table S1 in the Supporting Information) shows that the HF calculations predict a much lower energy than DFT, and the single-point calculations with the 6-311+G-(d,p) basis set are comparable with the B3LYP/6-31G(d) method. The relative energies of the isomers, transition states, and dissociation products obtained at the B3LYP/6-311+G-(d,p)//B3LYP/6-31G(d) level are shown in Figure 1.

Because the experiments and theoretical calculations suggest that the gauche conformer of neutral ethylene glycol is the most stable and the predominant conformer at room temperature,[2,9] only this conformer was calculated. Its relative energy is set to be zero, and the energies of all of the species in this study are relative to it. The structural parameters of neutral ethylene glycol obtained in this study are similar to the results obtained by other theoretical calculations.[7−12] In particular, one of the hydroxylic hydrogens points to the other O atom and forms a distorted intramolecular hydrogen bond.

A total of 13 different $C_2H_6O_2^{+\bullet}$ structures were obtained in this study, whose geometry and energies are shown in Figure S1 and Table S1 of the Supporting Information. The most important structures for this study are also shown in Figures 1a−c. Compound $\mathbf{1}^+$ corresponds to ionic ethylene glycol. The C−C bond is significantly extended from its neutral value of 1.521 Å to 1.850 Å, and no intramolecular hydrogen bond exists. Burgers et al.[19] obtained a $C_2H_6O_2^{+\bullet}$ ion structure at the Hartree−Fock level, which is similar to the neutral structure, and which includes an intramolecular hydrogen bond. Although, we also obtained such a structure at the HF/6-31G(d) level, all optimizations at the DFT (B3LYP) level converted this structure to $\mathbf{1}^+$. A large change in the geometry is consistent with our observation of a very gradual ionization onset and the broad peak observed in the photoelectron spectrum.

Structure $\mathbf{2}^+$ is obtained from $\mathbf{1}^+$ by a hydrogen transfer from O_4 to O_3. In this structure, the transferred H atom is only 1.656

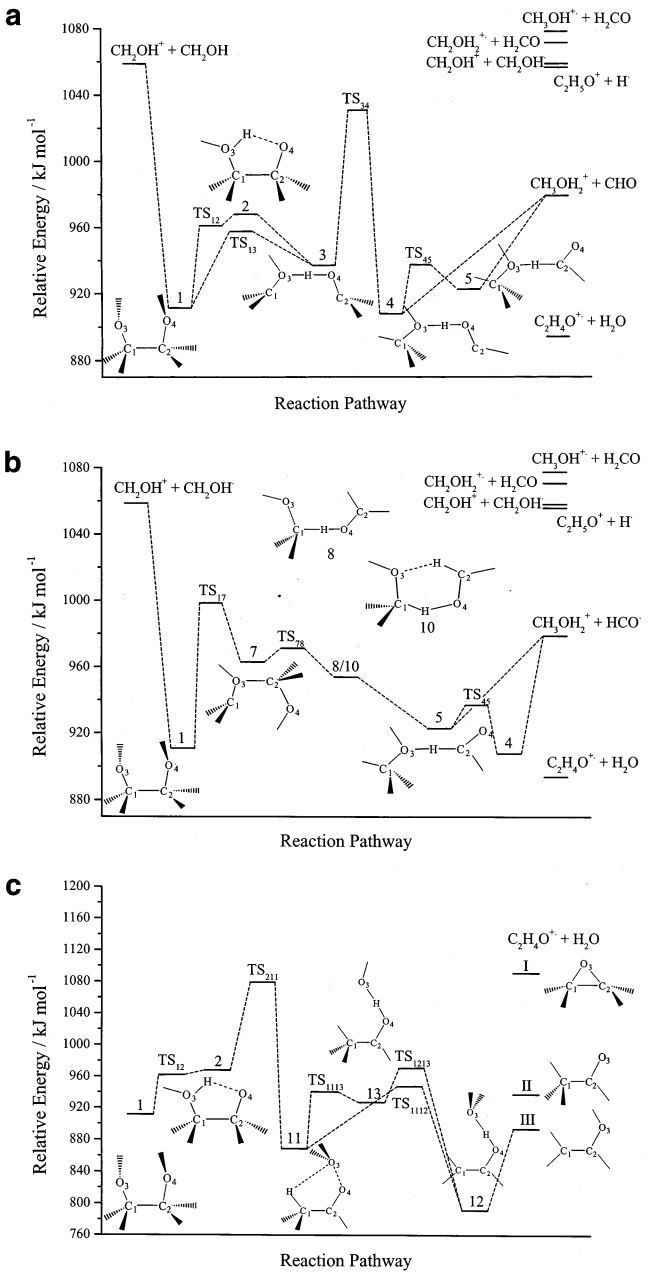

Figure 1. Energy diagram of the isomerization and dissociation reactions of the $C_2H_6O_2^{+\bullet}$ isomers. The energy is relative to the neutral ethylene glycol molecule. a. Mechanism I for the $CH_3OH_2^+$ ion production. b. Mechanism II for the $CH_3OH_2^+$ ion production. c. Mechanism for the $C_2H_4O^{+\bullet}$ ion production.

Å from O_4, qualifying this as a hydrogen bond. Structure $\mathbf{3}^+$ is the product of the C−C bond cleavage of $\mathbf{2}^+$, in which two CH_2OH groups connect together by an O−H···O hydrogen bond. Structure $\mathbf{4}^+$ is an ion−dipole complex between $CH_3OH_2^+$ and CHO•, connected by an O−H···O hydrogen bond. Structure $\mathbf{5}^+$ is the related complex in which the connecting linkage is an O−H−C bridge. Structure $\mathbf{7}^+$ in Figure 1b is obtained from $\mathbf{1}^+$ by a backbone rearrangement from O−C−C−O to O−C−O−C without an accompanying H atom transfer. Structures $\mathbf{8}^+$ and $\mathbf{9}^+$ are complexes between $CH_2O^{+\bullet}$ and CH_3OH, whereas $\mathbf{11}^+$, $\mathbf{12}^+$, and $\mathbf{13}^+$ (Figure 1c) are the three structures relevant to the $C_2H_4O^{+\bullet}$ ion production (H_2O loss reaction product). They will be discussed in the last section.

Mechanism I. The pathway associated with mechanism I is shown in Figure 1a. Burgers et al.[19] calculated the energy diagram of this mechanism at the Hartree−Fock level. They obtained the structures and energies of $\mathbf{1}^+$, $\mathbf{3}^+$, $\mathbf{4}^+$, and $\mathbf{6}^+$ and several dissociation channels but did not obtain the transition state structures. Thus, no information on the isomerization energy barrier heights is available.

The production of $CH_3OH_2^+$ involves the breakage of the C−C bond and two hydrogen transfer steps. The two probable precursors for CHO• loss are the ion−dipole complexes $\mathbf{4}^+$ and $\mathbf{5}^+$, which differ only in the orientation of the CHO• group. As shown in Figure 1a, the ethylene glycol ion, $\mathbf{1}^+$, can directly isomerize to $\mathbf{3}^+$ or pass to the intermediate structure, $\mathbf{2}^+$, and then produce $\mathbf{3}^+$. The major barrier in the reaction, located at 1031 kJ/mol, is the isomerization from $\mathbf{3}^+$ to $\mathbf{4}^+$ through a 1,5-H shift. The transition state connecting structures $\mathbf{4}^+$ and $\mathbf{5}^+$ is sufficiently low to permit these to be at equilibrium. The isomerization process from $\mathbf{3}^+$ to $\mathbf{4}^+$ is expected to be the rate-determining step. However, because the process involves hydrogen atom transfer, the tunneling effects could lower the experimentally observed energy barrier height.

Burgers et al.[19] suggested that an isomer with the structure $[H_3CO\cdots H\cdots OCH_2]^{+\bullet}$ ($\mathbf{6}^+$ in Figure S1 of the Supporting Information) can be produced from $\mathbf{4}^+$ by a 1,4-H shift. However, we could not obtain a transition state connecting $\mathbf{4}^+$ and $\mathbf{6}^+$. Instead, the very high-energy transition state, TS_{36}, is obtained. This corresponds to a hydrogen shift from oxygen to carbon.

Mechanism II. We also calculated stable structures and transition states along the potential energy surface associated with mechanism II (Figure 1b). This mechanism (eq 2) also involves a 1−2 and 1−5 H atom shift. However, these are preceded by an O atom insertion into the C−C bond. This insertion, which transforms O−C−C−O ($\mathbf{1}^+$) to O−C−O−C ($\mathbf{7}^+$), is followed by an isomerization to $\mathbf{8}^+$ through a 1,2-H shift from oxygen to carbon. Because of a relatively low energy barrier for a 1,5-H shift, $\mathbf{8}^+$ easily isomerizes to $\mathbf{5}^+$, which dissociates to $CH_3OH_2^+ + CHO^\bullet$. It should be noted that the above process is a somewhat different from the Audier mechanism in eq 2 in which isomer $\mathbf{7}^+$ rearranges via sequential 1,5- and 1,2-hydrogen shifts. That is, in eq 2, $\mathbf{7}^+$ isomerizes by a 1,5- hydrogen shift to $CH_3O(H)\text{-}CH_2O^{+\bullet}$ (structure $\mathbf{9}^+$ in the Supporting Information) rather than the $CH_2O{-}HCH_2OH^+$ (structure $\mathbf{8}^+$). The latter is 20 kJ/mol lower in energy than $\mathbf{9}^+$. We attempted to calculate the transition state connecting $\mathbf{7}^+$ and $\mathbf{9}^+$. However, all attempts to move the hydrogen atom from the terminal oxygen to the terminal carbon resulted in a rupture of the C−O bond so that a hydrogen-bridged complex ($\mathbf{8}^+$) is formed. Isomer $\mathbf{10}^+$ is similar to $\mathbf{8}^+$, in which the C−O−H−C−O−H atoms form a six-membered ring, with an energy 5 kJ/mol higher than $\mathbf{8}^+$.

It can be seen from Figure 1b that the highest energy barrier of this mechanism corresponds to the isomerization from $\mathbf{1}^+$ to $\mathbf{7}^+$ through TS_{17} (999 kJ/mol). This corresponds to the rearrangement process of the O−C−C−O backbone. Because no H atom transfer is involved, tunneling is not expected to play an important role in mechanism II. This is reflected in the critical frequencies for mechanisms I and II, which are 1720 and 808 cm^{-1}, respectively (Table 1).

1.2. Dissociation Channels and Dissociation Energies. Six dissociation channels shown in Figure 1 were calculated in this study. As discussed later, although the $C_2H_4O^{+\bullet} + H_2O$ channel (see Figure 1c) has the lowest dissociation energy, the channel has a high-energy barrier in the reaction pathway. According to the DFT calculations, the protonated methanol ($CH_3OH_2^+ + CHO^\bullet$), the hydrogen loss ($C_2H_5O_2^+ + H^\bullet$), and $CH_2OH^+ +$

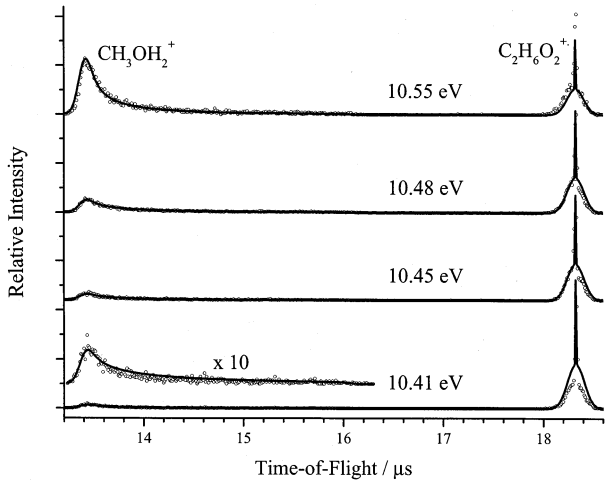

Figure 2. Ion TOF distributions at different photon energies. The points are the experimental data, and the solid lines are the simulation results.

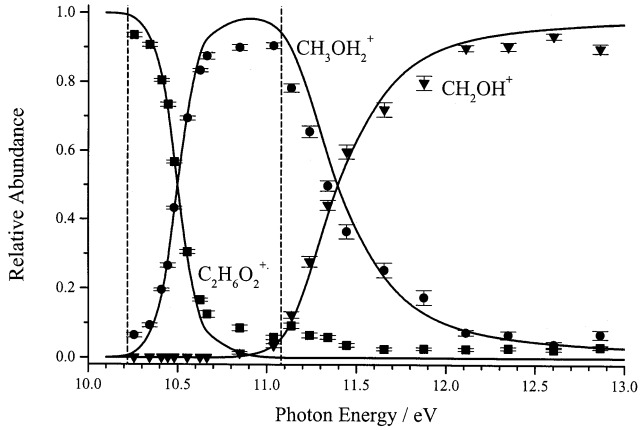

Figure 3. Breakdown diagram of the $C_2H_6O_2^{+\bullet}$ ion. The points are the experimental data with error estimates, and the solid lines are the simulation results. The dashed lines indicate the 0 K dissociation limits to the $CH_3OH_2^+ + CHO^\bullet$ and $CH_2OH^+ + CH_2OH^\bullet$ channels.

$CH_2OH^\bullet$ channels are the next three lowest energy dissociation channels. The hydrogen loss from the carbon atom (α cleavage) and the $CH_2OH^+ + CH_2OH^\bullet$ products are direct dissociation paths from the ethylene glycol ion, $\mathbf{1}^+$. These two channels have almost equal dissociation energies.

2. TPEPICO Experiments. 2.1. The Breakdown Diagram and TOF Distributions. The TOF mass spectra were collected in the photon energy range of 10.0 → 14.0 eV. Figure 2 shows typical low photon energy TOF distributions at which the $CH_3OH_2^+$ ion production reaction rates are slow. In the figure, the points are experimental data and the solid lines are the fitted TOF distributions (as discussed in the following section). The ion peak at about 18.3 μs, assigned to the parent ion, $C_2H_6O_2^{+\bullet}$ (*m*/*z* 62), consists of two parts, a central sharp peak on top of a broader one. The sharp part results from the effusive jet produced by the sample inlet, whereas the broad peak results from the background sample vapor. The simulation shows that the proportion from the effusive jet is about 5%. Although this is translationally cold, it probably has the same vibrational temperature as the background vapor. The breakdown diagram of the ethylene glycol ion between 10 and 13 eV is shown in Figure 3. The points are the experimental ratios with error estimates, and the solid lines are the simulation results. At photon energies below 10.7 eV, the protonated methanol ion (*m*/*z* 33) is the only product. At photon energies higher than

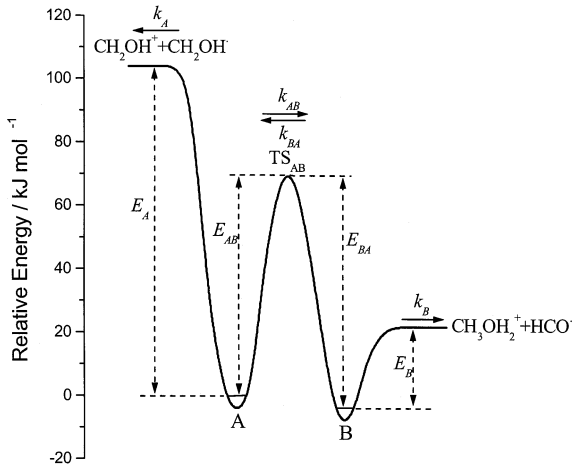

Figure 4. Two-well−two-channel model of the ethylene glycol dissociation and isomerization reactions. The energy scale is based on an adiabatic IE of ethylene glycol of 10.00 eV.

10.7 eV, a peak at *m*/*z* 31 is also observed, which corresponds to the direct C−C bond cleavage product of the ethylene glycol ion, CH_2OH^+ (+ $CH_2OH^\bullet$). The DFT calculations predict that the hydrogen loss and the $CH_2OH^+ + CH_2OH^\bullet$ channel should appear at about the same energy. However, at the photon energy higher than 10.7 eV, only a weak *m*/*z* 61 ion ($C_2H_5O_2^+$) peak (<5%) was found. This could be caused by a tight transition state and/or a centrifugal barrier associated with the H loss reaction thereby reducing its rate significantly relative to the $CH_2OH^\bullet$ loss channel.

At photon energies above 10.6 eV, a small amount of (<5%) the $C_2H_4O^{+\bullet}$ ion (*m*/*z* 44, H_2O loss product) was also found. Further analysis to determine its thermochemical onset was not attempted because of the weak signal. The $C_2H_4O^{+\bullet}$ ion production mechanism will be discussed in the last section.

In their collisional dissociation mass spectrometric study, Burgers et al.[19] noted the production of $CH_2OH_2^{+\bullet}$ (*m*/*z* 32), an ion that was not observed in our TPEPICO study. According to reasonably well established thermochemistry for all the species involved,[27] this channel is only about 70 meV more endothermic than the direct cleavage of the C−C bond to form CH_2OH^+. However, because it involves a rearrangement, it is rather surprising that it is produced in a high-energy collision induced dissociation process but not in the lower energy photoionization study.

As shown in Figure 2, at low photon energies between 10.3 and 10.7 eV, the peak shapes of the $CH_3OH_2^+$ ion TOF distributions are found to be asymmetric, which is a result of a slow ion dissociation in the first acceleration region. A careful modeling of the TOF distributions suggest that the rate is either two-component (a fast and a slow component) or that it is comprised of a broad distribution of rates. The latter situation arises when the rate varies very rapidly over the molecule's thermal energy distribution.

2.2. Simulation of the Experimental Data. As discussed above, two different reaction mechanisms have been suggested to describe the production of the protonated methanol ion. The potential energy surfaces depicted in Figure 1 parts a and b are clearly too complicated to model in detail. However, they can be simplified to a two-well model (Figure 4) in which TS_{34} or TS_{17} serve as the barrier (TS_{AB}) and structures $\mathbf{1}^+$ and $\mathbf{4}^+/\mathbf{5}^+$ serve as the isomerized wells (A and B). The rate constants and branching ratios can be modeled for such a two-well potential energy surface with the following rate equations: in

TABLE 2: Thermochemical Data (in kJ/mol)[a]

species	$\Delta_f H^\circ_{298K}$	$\Delta_f H^\circ_{0K}$	$H^\circ_{298K} - H^\circ_{0K}$ [b]	other results of $\Delta_f H^\circ_{298K}$
$C_2H_6O_2$	-383.1 ± 4.5[c]	-362.5 ± 4.5[d]	15.56	-394.4 ± 2.8,[e] -387.6 ± 1.7[f]
$C_2H_6O_2^{+\bullet}$(A)	582 ± 15[c]	602 ± 15[g]	16.38	593[f]
$C_2H_6O_2^{+\bullet}$(B)	584 ± 20[c]	599 ± 20[h]	20.90	—
$CH_3OH_2^+$	568.7 ± 3.0[i]	583.4 ± 3.0[j]	11.90	567[f]
$CHO^\bullet$	42.0 ± 4.0[e]	41.6 ± 4.0[j]	9.983[k]	44.8[f]
$CH_2OH^\bullet$	-17.8 ± 1.3[l]	-11.5 ± 1.3[l]	11.07	-9.0 ± 4.0,[e] -25.9,[f] -16.6 ± 0.9,[m] -16.6 ± 1.3,[n] -17.1 ± 3.3[o]
CH_2OH^+	710.2 ± 1.8[l]	718.1 ± 1.8[l]	10.14	718.0 ± 2.0,[e] 703,[f] 717.9 ± 0.7 (0 K)[m]

[a] In the $H^\circ_{298K} - H^\circ_{0K}$ calculations, the heat capacity of electron was treated as 0.0 kJ/mol at all temperatures (the ion convention[36]). To convert to the electron convention, which treats the electron as a real particle, 6.197 kJ/mol should be added to the 298 K heat of formation of each ion. [b] From the DFT calculated frequencies. [c] $\Delta_f H^\circ_{0K} \rightarrow \Delta_f H^\circ_{298K}$. [d] From the AE measurements, $\Delta_f H^\circ_{0K}(C_2H_6O_2) = \Delta_f H^\circ_{0K}(CH_2OH^+) + \Delta_f H^\circ_{0K}(CH_2OH^\bullet) - AE(CH_2OH^+)$ [e] Webbook.[37] [f] Gas-phase ion and neutral thermochemistry by Lias et al.[27] [g] $\Delta_f H^\circ_{0K}$(ion) = $\Delta_f H^\circ_{0K}$(neutral) + IE, where $IE(C_2H_6O_2) = 10.00$ eV and $IE(CH_2OH) = 7.56 \pm 0.01$ eV.[38] [h] $\Delta_f H^\circ_{0K}(C_2H_6O_2+, A) + \Delta E$, where $\Delta E = -3$ kJ/mol from the DFT calculation. [i] From $PA(CH_3OH) = 760.2$ kJ/mol,[39] $\Delta_f H^\circ_{298K}(CH_3OH) = -201.1 \pm 0.2$ kJ/mol[37] and $\Delta_f H^\circ_{298K}(H^+) = 1530.0$ kJ/mol.[37] [j] $\Delta_f H^\circ_{298K} \rightarrow \Delta_f H^\circ_{0K}$. [k] Reference 40. [l] Reference 41, $\Delta_f H^\circ_{298K}(CH_2OH^+)$ has been converted to the ion convention. [m] Reference 42. [n] Reference 43. [o] Reference 44.

$$\begin{aligned} d[A]/dt &= -(k_A + k_{AB})[A] + k_{BA}[B] \\ d[B]/dt &= k_{AB}[A] - (k_B + k_{BA})[B] \\ d[P_A]/dt &= k_A[A] \\ d[P_B]/dt &= k_B[B] \end{aligned} \tag{3}$$

which A and B refer to the two isomers of $C_2H_6O_2^{+\bullet}$, $\mathbf{1}^+$ and $\mathbf{4}^+$, P_A is the $CH_2OH^+ + CH_2OH^\bullet$ product channel, and P_B is the $CH_3OH_2^+ + CHO^\bullet$ product channel. The solutions of this system of equations are given below:

$$[A](t) = \alpha_1 \exp(-k_{fast}t) + \alpha_2 \exp(-k_{slow}t)$$

$$[B](t) = \frac{(k_{AB} + k_A - k_{fast})\alpha_1}{k_{BA}} e^{-k_{fast}t} + \frac{(k_{AB} + k_A - k_{slow})\alpha_2}{k_{BA}} e^{-k_{slow}t}$$

$$[P_B](t) = \frac{(k_{AB} + k_A - k_{fast})k_B\alpha_1}{k_{BA}k_{fast}}(1 - e^{-k_{fast}t}) + \frac{(k_{AB} + k_A - k_{slow})k_B\alpha_2}{k_{BA}k_{slow}}(1 - e^{-k_{slow}t})$$

$$[P_A](t) = \frac{k_A\alpha_1}{k_{fast}}(1 - e^{-k_{fast}t}) + \frac{k_A\alpha_2}{k_{slow}}(1 - e^{-k_{slow}t}) \tag{4}$$

in which k_{fast} and k_{slow} are the two roots of the following equation:

$$k_i^2 - (k_{AB} + k_{BA} + k_A + k_B)k_i + (k_{AB}k_B + k_{BA}k_A + k_Ak_B) = 0 \tag{5}$$

The parameters, α_1 and α_2, can be determined from the initial conditions, $[A](t = 0) = \alpha_1 + \alpha_2 = 1$ and $[B](t = 0) = 0$.

The rate constants k_A, k_B, k_{AB}, and k_{BA} in eq 5 can be calculated using statistical RRKM theory. Because the rate-limiting step in mechanism II involves the O−C−C−O backbone rearrangement without an H atom transfer, tunneling effects will not play a role. Thus, all of the rate constants are calculated using the formula[28]

$$k(E) = \frac{\sigma N^{\neq}(E - E_0)}{h\rho(E)} \tag{6}$$

in which E_0 is the activation energy, $N^{\neq}(E - E_0)$ is the sum of states of the transition state from 0 to $E - E_0$, and $\rho(E)$ is the density of states of the ion, respectively. σ is the symmetry parameter, which is 1 for the isomerizations between A and B and $CHO^\bullet$ loss reactions and is 2 for the $CH_2OH^\bullet$ loss reaction.

For mechanism I, the loss of $CHO^\bullet$ from the ethylene glycol ion involves a sequence of hydrogen atom rearrangements. Therefore, tunneling effects could play an important role, and the rate constants, k_{AB} and k_{BA}, which correspond to the isomerization processes between A and B, need to be calculated using RRKM theory with tunneling corrections:[28,29]

$$k(E) = \frac{\sigma}{h\rho(E)} \int_{-E_0}^{E-E_0} \kappa(\epsilon_t)\rho^{\neq}(E - E_0 - \epsilon_t)\, d\epsilon_t \tag{7}$$

in which $\rho^{\neq}(E)$ is the density of states of the transition state, ϵ_t is the translational energy in the reaction coordinate, and $\kappa(\epsilon_t)$ is the tunneling probability modeled with an Eckart barrier.[28]

The ion TOF distributions and the breakdown diagram were simulated by procedures described in previous publications.[30−32] Calculation of the ion TOF distribution and the breakdown diagram in Figures 2 and 3 involved a convolution over the room-temperature ethylene glycol thermal energy distribution and the electron energy resolution function for our TPEPICO experiment. Other fixed parameters were the acceleration electric fields, the acceleration, and drift field lengths. Because the heats of formation of CH_2OH^+, $CH_2OH^\bullet$, $CH_3OH_2^+$, and $CHO^\bullet$ are well established (see Table 2), the thermochemical dissociation limits were established based on these values. The heat of formation of ethylene glycol was treated as an adjustable parameter. The B well energy was taken from the DFT calculations because there are no experimental values for it. The adiabatic IE value of ethylene glycol is known much less accurately than the vertical IE of 10.55 eV. The Lias et al.[27] compilation lists an adiabatic IE of 10.16 eV, based on an old electron impact experiment.[33] Our measured threshold photoelectron spectrum and photoionization efficiency (PIE) curve showed no obvious ionization onset. We suggest an adiabatic IE of about 10.00 ± 0.15 eV with a large error limit that reflects the difficulty in assigning its value. Our DFT calculations indicate that the difference between the adiabatic and vertical IEs should be 0.834 eV, which combined with the experimental vertical IE yields an adiabatic IE of 9.72 eV. The large difference in the vertical and adiabatic IEs is a result of the large geometry change upon ionization. For the purposes of this study, we have rather arbitrarily chosen a value of 10.00 eV. It turns out that the final results are not very sensitive to the assumed IE value.

The assumed vibrational frequencies for isomers A and B shown in Table 1 were determined by DFT calculations of structures $\mathbf{1}^+$ and $\mathbf{4}^+$, respectively. The frequencies of TS_{AB} are those of TS_{34} or TS_{17} for mechanisms I and II, respectively.

Because mechanisms I and II involve a sequence of rearrangements, and the transition states TS_{34} and TS_{17} are only the highest energy barriers in the reaction pathways, the TS_{AB} frequencies need to be adjusted in order to fit the experimental results. TS_A and TS_B correspond to the dissociation of isomers A (structure $\mathbf{1}^+$) and B (structures $\mathbf{4}^+$ or $\mathbf{5}^+$), respectively. These are direct dissociation reactions without reverse activation energy barriers so that no unique transition state could be calculated. We thus approximated these frequencies by calculating the vibrational frequencies of structures $\mathbf{1}^+$ with the $HOH_2C\cdots CH_2$-$OH^{+\bullet}$ bond extended to 4.0 Å (TS_A) and of structure $\mathbf{4}^+$ with the $CH_3O(H)H^+\cdots OCH^\bullet$ bond also extended to 4.0 Å (TS_B). In fitting the model to the data, the major adjustable parameters were the five lowest frequencies in each of the three transition states, the energy barrier for TS_{AB}, and the critical (negative) frequency associated with the tunneling motion through TS_{AB}. Both the energy and the critical frequencies are inputs into the Eckart tunneling equation. These parameters were varied to obtain a best fit to the experimental data in Figures 2 and 3. The TOF distributions at low energies are sensitive to the magnitude of the rate constants and thus E_{AB} and the critical frequencies, whereas the breakdown diagram is sensitive to the ratio of rate constants at energies above the onset for the second dissociation channel.

To obtain an estimate of the errors associated with the derived energy parameters, the energy barrier height, the IE, and other energies were adjusted and held fixed (one at a time), whereas the rest of the parameters were allowed to vary for an optimum fit. These parameters were varied until the overall fit to the data worsened noticeably. In this manner, it was possible to not only determine the error limits on each parameter but also determine its effect on the simulation quality.

The simulation of the CH_2OH^+ onset was very sensitive to the assumed heat of formation of the ethylene glycol neutral molecule and did not depend very much on other parameters. Thus, the energy E_A in Figure 4 can be fixed at 1.08 ± 0.04 eV (assuming an IE of 10.00 eV), from which we obtain a $\Delta_f H^\circ_{298K}[C_2H_6O_2]$ of -383.1 ± 4.5 kJ/mol, which is very close to the accepted values that range from -387 to -394 kJ/mol. The only effect of varying the assumed adiabatic ionization energy of ethylene glycol was a corresponding variation in E_A, which kept their sum, IE + E_A, fixed at 11.08 eV.

Having fixed the value of E_A, the only remaining adjustable parameters were E_{AB}, a factor, f, which multiplied the five lowest frequencies of the transition state, TS_{AB}, and the factor, $f^\#$, which multiplied the critical (tunneling) frequency. The energies E_{BA} and E_B had no effect on the TOF distributions or the breakdown diagram because once the ion passed over TS_{AB} it reacted to products without returning to the A well. Thus, the B well was arbitrarily fixed at the value given by the DFT calculations, which is 4 kJ/mol below the A well. The data in Figures 2 and 3 could be fit by a range of assumed values for $f = 0.2 \rightarrow 5$, $f^\# = 0.8 \rightarrow 0.6$, and E_{AB} from 0.82 → 0.62 eV, respectively. The best fit was obtained with $f = 1.0$, $f^\# = 0.7$ ($\nu^\# = 1204$ cm^{-1}), and $E_{AB} = 0.72$ eV. The experimental E_{AB} of 0.72 eV can be compared to the calculated energy in two ways. The experimental TS_{AB} lies some 0.37 eV below the CH_2-$OH^+ + CH_2OH^\bullet$ dissociation limit. The DFT calculated energy difference between this dissociation limit and TS_{34} is 0.29 eV, which is within 8 kJ/mol, an excellent agreement by any standard. A nearly as good agreement (0.17 eV) between experiment and theory is associated with the energy difference between TS_{AB} (TS_{34}) and the other dissociation product. On the other hand, if we use the ethylene ground-state ion as the reference energy, then the experimental E_{AB} of 0.72 eV is far below the calculated one of 1.28 eV. The error seems to be associated with the DFT calculated ethylene glycol ion energy, which is too low.

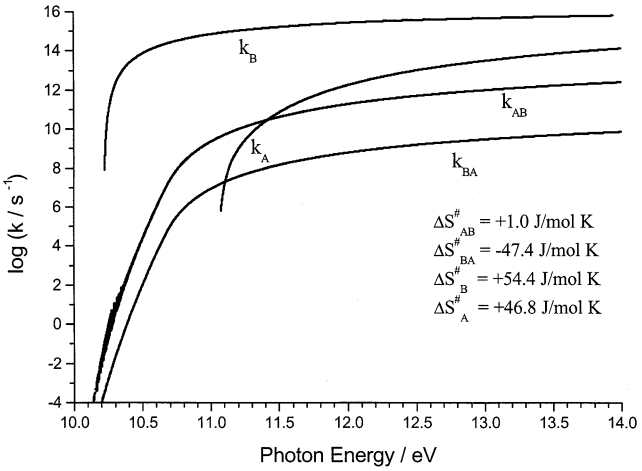

Figure 5. RRKM calculated rate curves and the activation entropies at 600 K for the four rate constants. Only k_A and k_{AB} affect the fit of the experimental data.

The RRKM calculated rate constant curves using the energies and frequencies that yielded the fit in Figures 2 and 3 are shown in Figure 5 along with the activation entropies for each channel. The rate constants, k_A and k_B, have large positive activation entropies, which indicates that the two reactions proceed via loose transition states. This is consistent with the fact that these two reactions are simple bond-cleavage reactions. On the other hand, the two isomerization rate constants, k_{AB} and k_{BA}, have either 0 or negative entropies of activation, again consistent with a tight transition state. Because these entropies involve the same transition state, the different values for $\Delta S^\#_{AB}$ and $\Delta S^\#_{BA}$ is ascribed to the much lower vibrational frequencies of B relative to A. This also explains the quantum oscillations in k_{AB} at low energies where the isomer A density of states is sparse. The rapid rise of k_A beginning at 11.08 eV accounts for the dominating contribution of the CH_2OH^+ signal at higher photon energies in Figure 3. The apparent "two-component" dissociation rates in this model are caused by the ethylene glycol thermal energy distribution that extends over 0.20 eV and the rapidly rising k_{AB} tunneling rate constants ($10^4 \rightarrow 10^7$ s^{-1}) over this small energy range. That is, the slow component is determined by the low energy ions, whereas the fast component is caused by the high-energy tail of the thermal energy distribution.

The simulations for mechanism II do not include tunneling. Thus, the slow observed rate constant can only be ascribed to the dissociation from a low energy isomer. That is, either the A well would have to be reduced by about 1 eV or the B well would have to be reduced by 2−3 eV. Such situations have been encountered before and give rise to two-component dissociation rates.[34,35] However, it was not possible to fit both the breakdown diagram and find a sufficiently low well to make the ethylene glycol ion metastable with respect to $CHO^\bullet$ loss. For instance, lowering the A potential well would also reduce the rate constant for the CH_2OH^+ ion production and thus result in a kinetic shift of this onset, which is inconsistent with the known thermochemistry of ethylene glycol and these products. We thus conclude that mechanism II does not account for our data because it does not involve a critical reaction step with tunneling.

We carried out one more test to verify that tunneling is responsible for the slow rate constant by measuring the

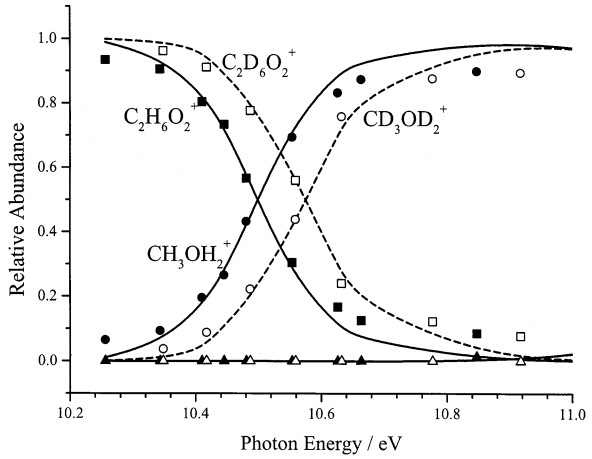

Figure 6. Comparison between the breakdown diagrams of $C_2H_6O_2^{+\bullet}$ and $C_2D_6O_2^{+\bullet}$. The points are the experimental data (solid symbols for normal and open symbols for deuterated samples), and the lines are the simulation results (solid line for normal and dashed line for deuterated samples).

breakdown diagram for deuterated ethylene glycol. As expected, the onset for the CH_2OH^+ ion, which is a simple C−C bond cleavage remained about the same, shifting to lower energy by at most 15 meV due to zero-point energy effects. However, as shown in Figure 6, the observed onset for the rearrangement reaction to produce $CH_3OH_2^+ + CHO^\bullet$ was shifted to higher energy by 80 meV. This is precisely the shift expected (dashed line) due to a reduced tunneling rate when D is substituted for H. The dashed line is generated with no additional fitting parameters, using energies determined in the fitting of the $C_2O_2H_6^+$ data and simply substituting the $C_2O_2D_6^+$ vibrational frequencies (Table 1). In particular, we used the same values for $\mathcal{f}$ and $\mathcal{f}^\#$, thereby making this a rather rigorous test of the tunneling hypothesis. The ratio of the critical frequency for the normal and deuterated sample for TS_{AB} (or TS_{34}) is 1.36, which is close to the expected value of 1.414 if this were a pure H atom transfer. On the other hand, the calculated ratio for TS_{17} in mechanism II is only 1.08, which is as expected for a transition state that does not involve an H atom transfer. More importantly, the transition state for mechanism II cannot account for the shift in the observed onset of the deuterated sample.

We are now left with a quandary. On one hand, our experimental results clearly indicate that tunneling is the only explanation for the slow dissociation rate, a result that appears to support mechanism I of Burgers et al.[19] and rule out mechanism II of Audier et al.[22] On the other hand, the isotopic labeling studies of Audier et al. clearly show that mechanism I is not valid because it does not yield the experimentally observed isotopically labeled products. To make matters worse, our DFT calculations of mechanism II indicate that the rate-limiting transition state, TS_{17} in mechanism II (Figure 1b) at an energy of 1000 kJ/mol relative to neutral ethylene glycol, corresponds precisely to the observed onset for $CH_3OH_2^+$ formation at 10.4 eV (1003 kJ/mol). That is, mechanism II predicts the correct onset energy for $CH_3OH_2^+$, but it does not account for the tunneling phenomenon and the shift in the deuterated sample nor the observation of a metastable parent ion as observed by us and by all MIKES studies of this ion. It may well be that mechanism II is important at somewhat higher energies but is not the mechanism near the threshold. One resolution of this paradox is to assume that the calculated TS_{17} energy is too low by at least 0.3 eV and the existence of yet a third mechanism, which does involve tunneling and is at the same time consistent with the isotopic labeling study. However, we have not been successful in generating such a mechanism.

An important issue is the robustness of the above conclusions. For instance, could a three-well model make the results consistent with mechanism II? We have worked with multiple well potential energy surfaces and have found that additional wells are important only if the barriers between wells are substantial. If the barriers are low, such as TS_{78} and TS_{45} in Figure 1b, the ions will equilibrate rapidly so that the whole system of wells acts as a single well, which is dominated by the lowest energy conformer, isomer $\mathbf{4}^+$ in this case. Thus, the energies of TS_{78} or TS_{45} would have to be raised by 30 and 60 kJ/mol, respectively, to affect the reaction dynamics. Even if this were done, it would still not explain the slow rate constant or the tunneling through an H atom transfer barrier. Another issue raised by these results, is the accuracy of the DFT calculations. We have taken the approach that vibrational frequencies are reasonably accurate, but that the energies, especially the transition state energies, contain considerable error. As listed in Table S1 of the Supporting Information, the calculated energy (relative to neutral ethylene glycol) of the $CH_2OH^+ + CH_2OH^\bullet$ products is 1056.5 kJ/mol, which compares well with the experimental value of 1068 kJ/mol. On the other hand, the same level of calculation yields an energy of 911 kJ/mol for the ethylene glycol ion, whereas the experimental energy is 965 ± 15 kJ/mol. It is clear from such comparisons that we must be cautious in relying too much on the accuracies of calculated ion energies. The situation is worse for transition state energies because few reactions have known transition states, whose experimental and calculated energies can be compared. Density functional theory has been optimized to yield accurate energies for stable molecules, not transition states. Thus, for the time being, we use calculated energies with caution and rely on the experimental results to provide the energies.

3. The Thermochemical Results. The 298 and 0 K thermochemical data of all relevant molecules and ions of this study are listed in Table 1, which also lists other available 298 K experimental or theoretical results. The heats of formation of $CH_2OH^\bullet$ and CH_2OH^+ are well determined on the basis of many different experimental and theoretical methods, which agree well with each other (see Table 2). Similarly, the heats of formation of $CH_3OH_2^+$ and $CHO^\bullet$ are also well-known. Because this study determines the appearance energy of the CH_2OH^+ ion, using the heats of formation of CH_2OH^+ and $CH_2OH^\bullet$, the 0 K heat of formation of the ethylene glycol molecule is determined to be −362.5 ± 4.5 kJ/mol. The 298 K heat of formation of the molecule can be derived to be −383.1 ± 4.5 kJ/mol using eq 8

$$\Delta_f H^\circ_{298K} - \Delta_f H^\circ_{0K} = [H^\circ_{298K} - H^\circ_{0K}] - [H^\circ_{298K} - H^\circ_{0K}](\text{elements}) \quad (8)$$

in which the $[H^\circ_{298K} - H^\circ_{0K}]$ values were calculated using vibrational frequencies obtained from the DFT calculations. The enthalpy changes of the elements in their standard states, $[H^\circ_{298K} - H^\circ_{0K}]$(elements), were calculated using the following values: C(s), 1.050 kJ/mol; H_2(g), 8.468 kJ/mol; and O_2(g), 8.680 kJ/mol.[40] This ethylene glycol heat of formation is in good agreement with the values listed in the Webbook[37] and the Gas-phase ion and neutral thermochemical compilation.[27] The latter two results are on the basis of the static bomb calorimetry measurements.[45] The 0 K heat of formation of ionic $C_2H_6O_2^{+\bullet}$ is obtained by adding $\Delta_f H^\circ_{0K}(C_2H_6O_2)$ and the adiabatic IE value of ethylene glycol (10.00 ± 0.15 eV). We could not

determine the heat of formation of the $C_2H_6O_2^{+\bullet}$ ($\mathbf{4}^+$) ion because our data are not sensitive to this energy. However, by combining the $\Delta_f H^\circ_{0K}$ ($C_2H_6O_2^{+\bullet}$, $\mathbf{1}^+$) and the DFT calculated energy difference between $\mathbf{1}^+$ and $\mathbf{4}^+$ (3 kJ/mol), a 298 K heat of formation of $\mathbf{4}^+$ is obtained to be 584 ± 20 kJ/mol.

4. The Production of $C_2H_4O^{+\bullet}$ (Loss of H_2O). The lowest energy products of the ethylene glycol ion dissociation is to $C_2H_4O^{+\bullet}$ (ethenol ion) + H_2O. However, the MIKES study[22] shows no $C_2H_4O^{+\bullet}$ ion production, and only a very weak *m*/*z* 44 peak was observed in the present experiments. This means that there are significant barriers for the water loss channel. As shown in Figure 1c, there are three possible isomers of the $C_2H_4O^{+\bullet}$ ion. The DFT calculated energies agree very well with those listed in the Webbook.[37] Although the highest energy ethylene oxide structure (I) can be directly produced from isomer 2, its energy is too high to compete with the lower energy channels in Figure 1 parts a and b. However, the other two structures, acetaldehyde (II) and ethenol or vinyl alcohol (III) have thermochemical onset energies below the $CH_3OH_2^+$ onset. However, their productions clearly require rearrangements. The complex between $CH_2{=}CHOH^{+\bullet}$ and H_2O has been experimentally observed, and its structure has also been suggested by ab initio calculations.[46] The calculations of Postma et al.[46] show that the hydrogen-bridged radical cation $[CH_2CHO\cdots H\cdots OH_2]^{+\bullet}$ ($\mathbf{12}^+$) has syn and anti isomers with comparable energies and an interconversion barrier of less than 10 kJ/mol. In this study, we only calculated the syn conformation. The Postma et al. dissociation energy (to $C_2H_4O^{+\bullet}$ + H_2O) is 85 kJ/mol for the syn conformation, which is slightly lower than 102 kJ/mol obtained by our DFT calculations. As shown in Figure 1c, the precursor ions for II and III are $\mathbf{12}^+$ and $\mathbf{11}^+$ (or $\mathbf{13}^+$), respectively. The production of $\mathbf{11}^+$ necessitates surmounting the transition state barrier, TS_{211}, which lies 48 kJ/mol higher than TS_{34}, and 20 kJ/mol higher than the CH_2OH^+ + $CH_2OH^\bullet$ channel. Thus, although structure $\mathbf{12}^+$ is the most stable of the $C_2H_6O_2^{+\bullet}$ isomers, it cannot be readily produced from ethylene glycol ions because of the high energy barrier separating the two structures.

Conclusions

The dissociation dynamics and thermochemistry of the ethylene glycol cation are investigated using the threshold photoelectron−photoion coincidence spectroscopy and density functional theory calculations. The breakdown diagram and time-of-flight distributions of the fragment ions, corresponding to the lowest two dissociation channels, $CH_3OH_2^+$ + $CHO^\bullet$ and CH_2OH^+ + $CH_2OH^\bullet$, are obtained. The $CH_3OH_2^+$ ion time-of-flight distributions are asymmetric indicating a slow dissociation to these products. A two-well−two-channel model is suggested to describe the dissociation-isomerization reactions of the ethylene glycol ion. The simulations of the experimental data for normal and deuterated ethylene glycol indicate that the production of the $CH_3OH_2^+$ ion proceeds by tunneling through a potential barrier associated with an H-atom transfer. Neither of the two previously suggested mechanisms for the ethylene glycol ion dissociation is consistent with these results. Although mechanism I accounts for the slow $HCO^\bullet$ loss rate constant, it is apparently not consistent with H,D deuterium labeling studies. Mechanism II accounts for the labeling results but does not account for the slow rate constant and the tunneling observed in our PEPICO study. By combining the derived dissociation limit with the known heats of formation of the $CH_2OH^+/CH_2OH^\bullet$ products, the 298 K ethylene glycol heat of formation is determined to be −383.1 ± 4.5 kJ/mol.

Acknowledgment. We thank the North Carolina Supercomputer facility for a generous allotment of computer time. This work was supported by a grant from the U.S. Department of Energy, Office of Basic Energy Sciences.

Supporting Information Available: A table of the DFT calculated energies (Table S1) and a figure of all the structures and transition states (Figure S1). This material is available free of charge via the Internet at http://pubs.acs.org.

References and Notes

(1) Bastiansen, O. *Acta Chem. Scand.* **1949**, *3*, 415.
(2) Frei, H.; Ha, T. K.; Meyer, R.; Gunthard, H. H. *Chem. Phys.* **1977**, *25*, 271.
(3) Buckley, P.; Giguère, P. A. *Can. J. Chem.* **1967**, *45*, 397.
(4) Kristiansen, P. E.; Marstokk, K. M.; Mollendal, H. *Acta Chem. Scand.* **1987**, *A41*, 403.
(5) Caminati, W.; Corbelli, G. *J. Mol. Spectrosc.* **1981**, *90*, 572.
(6) Walder, E.; Bander, A.; Günthard, H. H. *Chem. Phys.* **1980**, *51*, 223.
(7) Csonka, G. I.; Anh, N.; Angyan, J.; Csizmadia, I. G. *Chem. Phys. Lett.* **1995**, *245*, 129.
(8) Oie, T.; Topol, I. A.; Burt, S. K. *J. Phys. Chem.* **1994**, *98*, 1121.
(9) Cramer, C. J.; Truhlar, D. G. *J. Am. Chem. Soc.* **1994**, *116*, 3892.
(10) Nagy, P. I.; Dunn, W. J. I.; Alagona, G.; Ghio, C. *J. Am. Chem. Soc.* **1992**, *114*, 4752.
(11) Murcko, M. A.; DiPaola, R. A. *J. Am. Chem. Soc.* **1992**, *114*, 10010.
(12) Nagy, P. I.; Dunn, W. J. I.; Alagona, G.; Ghio, C. *J. Am. Chem. Soc.* **1991**, *113*, 6719.
(13) Ohno, K.; Imai, K.; Harada, Y. *J. Am. Chem. Soc.* **1985**, *107*, 8078.
(14) Niessen, W. V.; Bieri, G.; Asbrink, L. *J. Electron Spectrosc. Relat. Phenom.* **1980**, *21*, 175.
(15) Kimura, K.; Katsumata, S.; Achiba, Y.; Yamazaki, T.; Iwata, S. *Handbook of He(I) Photoelectron Spectra of Fundamental Organic Molecules*; Halsted Press: New York, 1981.
(16) Holmes, J. L.; Lossing, F. P. *Int. J. Mass Spectrom. Ion. Proc.* **1984**, *58*, 113−120.
(17) Holmes, J. L.; Lossing, F. P.; Terlouw, J. K.; Burgers, P. C. *Can. J. Chem.* **1983**, *61*, 2305.
(18) Holmes, J. L.; Lossing, F. P.; Terlouw, J. K.; Burgers, P. C. *J. Am. Chem. Soc.* **1982**, *104*, 2931.
(19) Burgers, P. C.; Holmes, J. L.; Hop, C. E. C. A.; Postma, R.; Ruttink, P. J. A.; Terlouw, J. K. *J. Am. Chem. Soc.* **1987**, *109*, 7315.
(20) Biermann, H. W.; Morton, T. H. *J. Am. Chem. Soc.* **1983**, *105*, 5025.
(21) Morton, T. H. *Tetrahedron* **1982**, *38*, 3195.
(22) Audier, H. E.; Milliet, A.; Leblanc, D.; Morton, T. H. *J. Am. Chem. Soc.* **1992**, *114*, 2020.
(23) Frisch, M. J.; Trucks, G. W.; Schlegel, H. B.; Scuseria, G. E.; Robb, M. A.; Cheeseman, J. R.; Zakrzewski, V. G.; Montgomery, J. A., Jr.; Stratmann, R. E.; Burant, J. C.; Dapprich, S.; Millam, J. M.; Daniels, A. D.; Kudin, K. N.; Strain, M. C.; Farkas, O.; Tomasi, J.; Barone, V.; Cossi, M.; Cammi, R.; Mennucci, B.; Pomelli, C.; Adamo, C.; Clifford, S.; Ochterski, J.; Petersson, G. A.; Ayala, P. Y.; Cui, Q.; Morokuma, K.; Malick, D. K.; Rabuck, A. D.; Raghavachari, K.; Foresman, J. B.; Cioslowski, J.; Ortiz, J. V.; Stefanov, B. B.; Liu, G.; Liashenko, A.; Piskorz, P.; Komaromi, I.; Gomperts, R.; Martin, R. L.; Fox, D. J.; Keith, T.; Al-Laham, M. A.; Peng, C. Y.; Nanayakkara, A.; Gonzalez, C.; Challacombe, M.; Gill, P. M. W.; Johnson, B. G.; Chen, W.; Wong, M. W.; Andres, J. L.; Head-Gordon, M.; Replogle, E. S.; Pople, J. A. *Gaussian 98*, revision A.7; Gaussian, Inc.: Pittsburgh, PA, 1998.
(24) Peng, C.; Schlegel, H. B. *Isr. J. Chem.* **1994**, *33*, 449.
(25) Peng, C.; Ayala, P. Y.; Schlegel, H. B.; Frisch, M. J. *J. Comput. Chem.* **1996**, *17*, 49.
(26) Baer, T.; Booze, J. A.; Weitzel, K. M. Photoelectron photoion coincidence studies of ion dissociation dynamics. In *Vacuum ultraviolet photoionization and photodissociation of molecules and clusters*; Ng, C. Y., Ed.; World Scientific: Singapore, 1991; pp 259.
(27) Lias, S. G.; Bartmess, J. E.; Liebman, J. F.; Holmes, J. L.; Levin, R. D.; Mallard, W. G. *Gas-Phase Ion and Neutral Thermochemistry*, *J. Phys. Chem. Ref. Data Vol 17, suppl. 1*; NSRDS: U.S. Government Printing Office: Washington, DC, 1988.
(28) Baer, T.; Hase, W. L. *Unimolecular Reaction Dynamics*: *Theory and Experiments*; Oxford University Press: New York, 1996.
(29) Miller, W. H. *J. Am. Chem. Soc.* **1979**, *101*, 6810.
(30) Li, Y.; Baer, T. *Int. J. Mass Spectrom.* **2002**, *218*, 19.
(31) Li, Y.; Baer, T. *Int. J. Mass Spectrom.* **2002**, *218*, 37.
(32) Oliveira, M. C.; Baer, T.; Olesik, S.; Almoster Ferreira, M. A. *Int. J. Mass Spectrom. Ion. Proc.* **1988**, *82*, 299.
(33) Holmes, J. L.; Lossing, F. P. *Can. J. Chem.* **1982**, *60*, 2365.

(34) Mazyar, O. A.; Baer, T. *J. Phys. Chem. A* **1998**, *102*, 1682.
(35) Mazyar, O. A.; Mayer, P. M.; Baer, T. *Int. J. Mass Spectrom. Ion. Proc.* **1997**, *167*/*168*, 389.
(36) Rosenstock, H. M.; Draxl, K.; Steiner, B. W.; Herron, J. T. *J. Phys. Chem. Ref. Data Vol. 6. Energetics of gaseous ions*; American Chemical Society: Washington, DC, 1977.
(37) http://webbook.nist.gov/chemistry/om/. 2000.
(38) Dyke, J. M.; Ellis, A. R.; Jonathan, N.; Keddar, N.; Morris, A. *Chem. Phys. Lett.* **1984**, *111*, 207.
(39) Szulejko, J. E.; McMahon, T. B. *J. Am. Chem. Soc.* **1993**, *115*, 7839.
(40) Wagman, D. D.; Evans, W. H. E.; Parker, V. B.; Schum, R. H.; Halow, I.; Mailey, S. M.; Churney, K. L.; Nuttall, R. L. *The NBS Tables of Chemical Thermodynamic Properties*, *J. Phys. Chem. Ref. Data Vol. 11 Suppl. 2*; NSRDS; U.S. Government Printing Office: Washington, CD, 1982.
(41) Johnson, R. D., III.; Hudgens, J. W. *J. Phys. Chem.* **1996**, *100*, 19874.
(42) Ruscic, B.; Berkowitz, J. *J. Phys. Chem.* **1993**, *97*, 11451.
(43) Dobe, S.; Berces, T.; Turanyi, T.; Marta, F.; Grussdorf, J.; Temps, F.; Wagner, H. G. *J. Phys. Chem.* **1996**, *100*, 19864.
(44) Berkowitz, J.; Ellison, G. B.; Gutman, D. *J. Phys. Chem.* **1994**, *98*, 2744.
(45) Gardner, P. J.; Hussain, K. S. *J. Chem. Thermodyn.* **1972**, *4*, 819.
(46) Postma, R.; Ruttink, P. J. A.; van Duijneveldt, F. B.; Terlouw, J. K.; Holmes, J. L. *Can. J. Chem.* **1985**, *63*, 2798.